Boosting Short-Circuit Current Density and Infrared Absorption in P3HT:PCBM Solar Cells with Plasmonic Aluminum Nanocylinders

Nasrin Sepahvand[a], Abdolmohammad Ghalambor Dezfuli[a,b,*], Mohsen Bahrami[c]
[a]Department of Physics, Faculty of Science, Shahid Chamran University of Ahvaz, Ahvaz, Iran
[b]Center for Research on Laser and Plasma, Shahid Chamran University of Ahvaz, Ahvaz, Iran
[c]Department of Physics, Faculty of Science, Lorestan University, Khorramabad, Iran

***Corresponding author email:** a.ghalambor@scu.ac.ir

Received: Sept. 21, 2025, Revised: Apr. 13, 2026, Accepted: Apr. 25, 2026, Available Online: Apr. 30, 2026.
DOI: Due to the current conditions, there is no possibility to buy DOI for papers. We hope to buy them as soon as possible.

ABSTRACT- Advancements in light-based technologies necessitate the development of optoelectronic devices for future renewable energy applications. A key challenge in enhancing the efficiency of organic solar cells (OSCs) lies in improving light absorption in the near-infrared (NIR) region, where conventional organic materials, such as P3HT[1]:PCBM[2], suffer from inherently weak absorption. In this study, we introduce a hexagonal periodic array of aluminum (Al) nanocylinders as a low-cost and effective plasmonic platform to address this limitation. Using finite-difference time-domain (FDTD) simulations, we optimized the nanostructure embedded within the P3HT:PCBM active layer. The proposed design excites strong localized surface plasmon resonances (LSPRs), leading to a significant enhancement in near-field intensity and effective optical path length, particularly across the 650–1200 nm spectrum. Through systematic optimization of nanocylinder dimensions (height: 50 nm, radius: 15 nm) and array periodicity (21 nm), an optimal active layer thickness of 150 nm was identified. The resulting plasmonic OSC achieves an optical upper bound short-circuit current density (J_{SC}) of 36.04 mA/cm^2, representing a twofold enhancement over the reference cell. These results highlight the potential of aluminum nanocylinders as an effective plasmonic platform for enhancing light absorption in organic solar cells.

KEYWORDS: Aluminum nanocylinders, FDTD, Light trapping, Near-infrared absorption, Organic solar cells, Plasmonics.

I. INTRODUCTION

The utilization of solar energy through photovoltaic technology has witnessed remarkable progress in recent decades [1], [2]. Among various types of solar cells, organic photovoltaics (OPVs) have attracted significant attention due to their compelling advantages, including light weight, mechanical flexibility, ease of fabrication, and potential for low-cost production [3]-[7]. A major limitation of organic active materials is their inherently weak light absorption, leading to significantly lower power conversion efficiencies compared to their inorganic counterparts, such as silicon solar cells [8].

This weak absorption, combined with the low charge carrier mobility (approximately 10^{-4}cm^{2}V^{-1}s^{-1}) and short exciton diffusion lengths in organic semiconductors, necessitates the use of thin active layers (typically less than 200 nm) [9], [10]. While this minimizes charge

[1] Poly(3-hexylthiophene)

[2] Fullerene derivative -phenyl-C61-butyric acid methyl ester

recombination losses, it inherently limits photon absorption capacity. This creates a fundamental trade-off between optical absorption and electrical transport, resulting in suboptimal power conversion efficiencies [11], [12]. Therefore, a central challenge in OPV design is to enhance light absorption within the intrinsically thin active layer.

A promising strategy to overcome this trade-off is to increase the effective light path length and boost light-matter interaction of the active layer. Plasmonic nanostructures have emerged as a particularly effective solution for this purpose, as they can confine light at the nanoscale and dramatically enhance the optical field within the semiconductor [13]. Specifically, the integration of metallic nanoparticles (NPs) to excite localized surface plasmon resonance (LSPR) modes has proven highly effective for light trapping [14, 15]. LSPRs are coherent oscillations of conduction electrons at the metal-dielectric interface, occurring when the frequency of incident light matches the natural frequency of these electrons [17, 18]. LSPRs lead to strong near-field enhancement and increased optical scattering, thereby boosting the effective light path length within the semiconductor layer [16]. The characteristics strongly depend on the nanoparticle material, geometry, and surrounding dielectric environment [18]. Noble metals like silver (Ag) and gold (Au) have been widely used due to their strong plasmonic responses in the visible spectrum. However, Ag nanoparticles suffer from oxidation issues, while the high cost of Au limits their practical application [19]-[21]. In recent years, aluminum (Al) has emerged as a highly promising alternative plasmonic material. Al offers compelling advantages: it is Earth-abundant, low-cost, and exhibits tunable plasmon resonances across a broad range, from the ultraviolet (UV) to the near-infrared (NIR) [22], [23]. Crucially, its inter-band transitions around 1.5 eV enable strong plasmonic activity in the NIR region [23], making it exceptionally suitable for enhancing solar cells where harvesting low-energy photons is critical.

Previous studies have extensively explored the use of various metallic nanostructures to enhance light absorption in OPVs [24]–[26]. Tseng, *et al.* investigated the dependence of light absorption on the shape and size of gold nanocrystals in bulk heterojunction solar cells [27], while Hsiao, *et al.* used gold nanostructures of different sizes to improve absorption [28]. Similarly, other groups have reported enhanced absorption by optimizing nanoparticle dimensions [29], [30]. Notably, Rodriguez, *et al.* highlighted the light-trapping potential of aluminum nanopyramids, underscoring the promise of non-spherical Al nanostructures [31]. Despite these efforts, research has predominantly focused on noble metal nanoparticles (e.g., Au and Ag) or isolated Al nanostructures with specific geometries. However, the potential of highly ordered, periodic arrays of aluminum nanocylinders, specifically for boosting NIR absorption in P3HT:PCBM-based solar cells, remains largely unexplored. P3HT:PCBM, a benchmark organic blend, has a bandgap of ~1.9 eV, limiting its effective light absorption to wavelengths below 650 nm [32]. Consequently, it fails to harvest photons in the NIR spectral region (700 nm–1200 nm), which accounts for nearly half of the sun's energy [33]. This results in the utilization of only ~22.4% of the total photons in the AM1.5G solar spectrum [32].

To address this challenge, we propose and numerically investigate a novel design incorporating a hexagonal periodic array of aluminum nanocylinders into the P3HT:PCBM active layer. The primary objectives of this work are: (1) to numerically optimize the plasmonic structure, including nanocylinder dimensions and array periodicity, for maximum broadband absorption enhancement, particularly in the NIR region (650 nm– 1200 nm); (2) to determine the optimal active layer thickness that balances enhanced optical absorption with efficient electrical transport in the presence of the plasmonic array; and (3) to maximize the short-circuit current density (J_{sc}) as a key performance indicator. By fulfilling these objectives, this work aims to establish aluminum nanocylinders as a low-cost,

scalable, and highly effective plasmonic platform for next-generation, high-efficiency organic solar cells (OSCs).

II. THEORY AND METHOD

The structure of the studied solar cell is schematically illustrated in Fig. 1(a). Indium tin oxide (ITO) serves as the anode electrode and hole collector, and its high conductivity also enables it to function as an anti-reflective coating (thickness: 178 nm), minimizing light reflection and optical losses for s-polarized incident radiation [34]. A 50 nm-thick layer of PEDOT[1]:PSS[2] acts as the hole transport layer, exhibiting high conductivity and a charge carrier mobility of 18.45 $cm^2V^{-1}s^{-1}$ [34], [35]. The active layer consists of the P3HT:PCBM blend, where P3HT functions as the electron donor (p-type polymer), and PCBM, a fullerene derivative, serves as the electron acceptor (n-type polymer) [17], [36]; the thickness of this layer is optimized during simulation. The remaining components include a 70 ɲm-thick zinc oxide (ZnO) layer (refractive index ≈ 1.4) acting as an electron-transporting and hole-blocking layer [37], and a 200 nm-thick Al layer serving as the cathode electrode and electron collector [35]. As shown in Fig. 1(b), the aluminum nanocylinders are arranged in a hexagonal pattern at the interface between the active layer (P3HT:PCBM) and the electron transport layer (ZnO).

In contrast to many previous studies that assume fixed, wavelength-independent refractive indices for OSC layers, this study employs wavelength-dependent complex refractive indices for all materials to ensure greater physical accuracy. As sunlight spans a broad spectral range (300 nm–1200 nm), accounting for the dispersive optical properties of each layer is essential for reliable modeling. Figure 2 presents the real (n) and imaginary (*k*) parts of the refractive index for ITO, PEDOT:PSS, P3HT:PCBM, ZnO, and Al across this range. As shown in Fig. 2(a), the real part of the refractive index for dielectric materials (ITO, PEDOT:PSS, ZnO) generally decreases with increasing wavelength. More importantly, Fig. 2(b) reveals that the imaginary part (*k*), which governs optical absorption, is nearly zero for ITO, PEDOT:PSS, and ZnO throughout the 300 nm–1200 nm range, confirming their roles as optically transparent transport layers. In contrast, the P3HT PCBM active layer exhibits significant absorption (k>0) up to ~650 nm, corresponding to its bandgap of 1.9 eV. This strong absorption coefficient facilitates efficient exciton generation upon photon absorption.

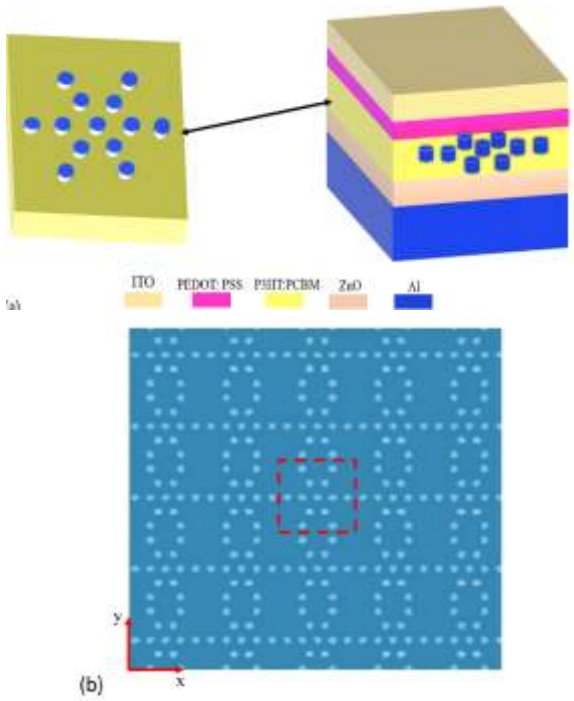

Fig. 1. (a) Schematic structure of the organic solar cell, ITO/PEDOT:PSS/P3HT:PCBM/ZnO/Al, along with an image of a cell of nanoparticles. (b) The placement pattern of nanocylinders inside the P3HT:PCBM layer of the solar cell.

Solving Maxwell's equations can be used to calculate the amount of light absorption in different layers of OSC. By calculating the distribution of the electric field in the OSC structure, the absorbed power per unit volume and wavelength unit is expressed as follows [38]:

[1] Poly(3,4-ethylenedioxythiophene)

[2] Polystyrene sulfonate

$$P_{abs}(r.\lambda) = -\frac{1}{2}\text{Real}(i\omega\varepsilon(r.\lambda)|E(r.\lambda)|^2) = \frac{1}{2}\omega|E(r.\lambda)|^2\text{Im}(\varepsilon(r.\lambda)) \quad (1)$$

where $|E(r.\lambda)|^2$ expresses the intensity of the electric field, depending on the frequency, and its unit is V^2/m^2Hz. The $\text{Im}(\varepsilon(r\ \lambda))$ is the imaginary part of the dielectric function for each layer, and ω is the angular frequency of the incident electric field. λ and r are the wavelength and position vectors, respectively. Wavelength-dependent Optical absorption, $L(\lambda)$, can be calculated by normalizing the power absorbed by the material to the power of the source [42]:

$$L(\lambda) = \frac{P_{abs}}{P_{sorce}} = \frac{1}{P_{sorce}}\int\frac{1}{2}\omega|E(r.\lambda)|^2\text{Im}\big(\varepsilon(r.\lambda)\big)dV \quad (2)$$

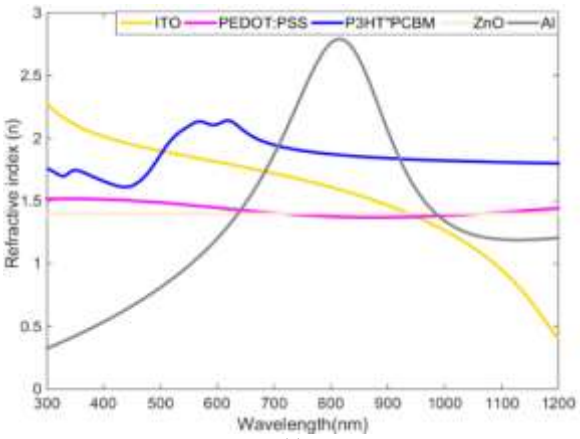

(a)

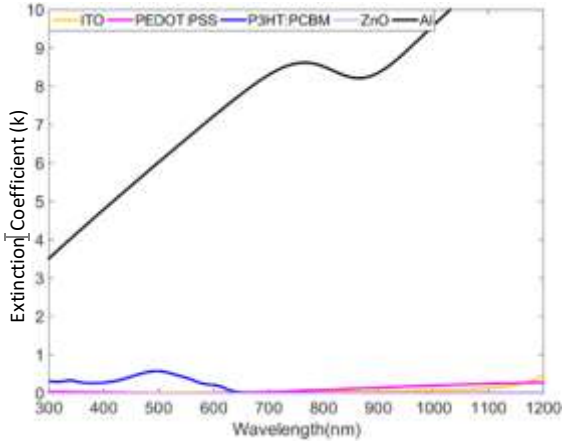

(b)

Fig. 2. (a) real, and (b) imaginary parts of the refractive index spectra of (1) ITO, (2) PEDOT:PSS, (3) P3HT:PCBM, (4) ZnO, (5) Al.

Figure 3 shows the absorption spectrum of ITO, PEDOT:PSS, ZnO, and Al layers in the specified thicknesses. The results indicate that ZnO is also a transparent layer. Therefore, it is necessary to choose a thick Al layer coating with thin layers of ITO and PEDOT:PSS to design a solar cell with high absorption in the active layer. The optimal thickness of the P3HT:PCBM active layer is obtained in the next part of the calculations.

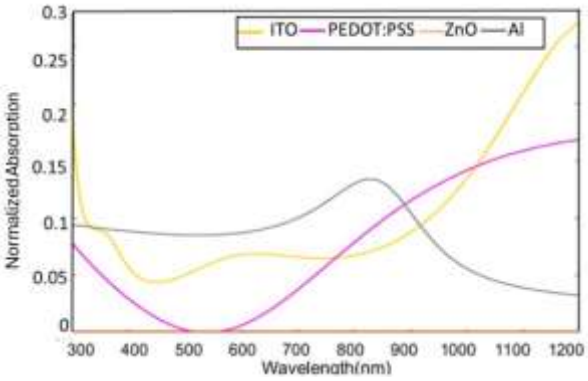

Fig. 3. Absorption spectra of ITO (178 nm), PEDOT:PSS (50 nm), ZnO (70 nm), and Al (500 nm) layers in certain thicknesses.

The short circuit current density (J_{SC}) shows the amount of electric current produced in the OSC at a voltage equal to zero (short circuit). In other words, this quantity depends on the photon flux that enters the OSC structure by the incident light spectrum and is calculated as follows [39]:

$$J_{sc} = q\int_{0.3}^{1.2}\frac{IAM1.5G(\lambda)}{\lambda}\cdot L(\lambda)d\lambda \quad (3)$$

where, $IAM1\text{-}5G(\lambda)$ is the spectral irradiance of the standard AM1.5G solar spectrum, and q is the elementary charge. This equation is proportional to the change in the amount of light absorbed by the nanoparticles, which shows how the nanoparticles excite the electrons around them [43]. It should be noted that this expression assumes ideal external quantum efficiency (EQE=100%) and complete carrier collection. Based on the limit of plasmonic resonance of metal nanoparticles (visible-infrared) and also the radiation spectrum of the sun, standard AM1.5G has been selected as the Integral limit in the wavelength range of 300 to 1200 nm. The absorption in the thin layer of semiconductors is low due to their energy gap (Fig. 3). Therefore, by placing metal nanoparticles in OSC structures, a dipole field is created on their surface. This field leads to the creation of strong near fields, increasing the scattering (σ_{sc}) and absorption σ_{abs} cross-

sections of incident light by trapping light through surface plasmons in OSC structures. If the size of the metal nanoparticles is smaller than or equal to the wavelength of the incident light, the surface of σ_{sc} and σ_{abs} cross sections can be calculated in the quasi-static approximation through the following equations [44]:

$$\sigma_{sc} = \frac{1}{6\pi}\left(\frac{2\pi}{\lambda}\right)^4 |\alpha|^2 = {}^{8\pi}/_{3}\, k^4 a^6 \left(\frac{\varepsilon_m - \varepsilon_d}{\varepsilon_m + 2\varepsilon_d}\right) \quad (4)$$

$$\sigma_{abs} = \frac{2\pi}{\lambda} \mathrm{I}M(\alpha) = 4\pi k a^3 \mathrm{Im}\left(\frac{\varepsilon_m - \varepsilon_d}{\varepsilon_m + 2\varepsilon_d}\right)^2 \quad (5)$$

with

$$\alpha = 3V\left[\frac{{}^{\varepsilon_d}/_{\varepsilon_m} - 1}{{}^{\varepsilon_d}/_{\varepsilon_m} + 2}\right] \quad (6)$$

where α and V represent polarizability and nanoparticle volume, respectively. ε_d and ε_m are the dielectric functions of the nanoparticle and the surrounding environment, respectively. If $\varepsilon_d = -2\varepsilon_m$, the polarizability of nanoparticles becomes very large. This occurs when the frequency of the incident light is close to the surface plasmon resonance (ω_{sp}), which allows the light to interact with the nanoparticle in an area larger than its geometric cross-section [41]. Based on the above equations, metal nanoparticles can act as either scattering amplifiers or localized electric fields, depending on their sizes. On the other hand, when nanoparticles are placed in the active layer, the exciton production rate can also increase proportionally to the square of the substitution field increase factor:

$$G\alpha P = \frac{1}{2}\varepsilon'' \omega |E|^2 \quad (7)$$

where G is the exciton generation rate, P is the electromagnetic energy loss rate, ε'' is the imaginary part of the dielectric function of the active layer, ω is the angular frequency of the electromagnetic wave, and E is the alternating electric field. Before the manufacturing process, designing and analyzing a solar cell play an important role in predicting its optical parameters. Choosing a suitable analytical method for a solar cell is challenging due to the complexity of the structure, such as the number of layers, different geometries, and the materials used for each layer.

In this study, we use the FDTD numerical method to calculate the above quantities. This method directly solves Maxwell's rotation equations, i.e., equations related to Ampere's and Faraday's laws, and does not need to define potentials. In this method, according to Fig. 4(a), the simulation space is divided into cubic cells (Yee's cell). The grid algorithm is a starting point for calculations based on the finite difference method in the time domain. As the figure shows, in this method, the wave vectors of the produced electric and magnetic fields are expanded, and the components of the magnetic field are half a unit length away from the electric field. Considering the central difference approximation for both temporal and spatial derivatives of Maxwell's equations, this method directly measures all electric field and magnetic field components in all three spatial dimensions of the computational range (x, y, z) [42]. During calculations, we expose the OSC structure to the radiation of a plane wave light source (TE- transverse electric mode).

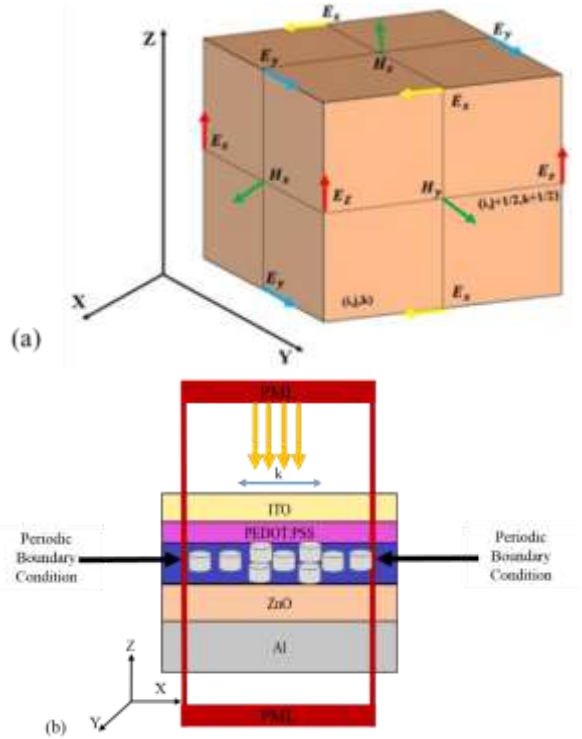

Fig. 4. (a) Yee's computational cell. (b) Side view of the unit cell of the simulation model in the x-z plane,

including perfectly matched layers (PML) and periodic boundary conditions.

According to Fig. 4(b), in the upper and lower boundaries of the simulation area, i.e., the z direction, to avoid creating unrealistic reflections from the borders, the perfectly matched layer (PML) boundary condition was applied. At the lateral boundaries (x and y directions), periodic boundary conditions are applied because the desired simulation structure is periodic in these directions. Since direct simulation of the entire solar cell takes a lot of time, we chose a single cell and repeated it in both x and y directions to simulate the entire structure more easily.

All FDTD simulations were performed using Lumerical FDTD Solutions (Ansys Inc., version 2022 R2). The maximum mesh pitch (point-to-point distance) in all directions was set to dx=dy=dz=0.1 nm to accurately capture plasmonic near-field enhancements. All photocurrent calculations are performed under standard AM1.5G incident with spectral integration limits of 300–1200 nm, covering the absorption range of P3HT:PCBM and plasmonic resonances of Al nanocylinders.

III. Results and Discussion

As stated above, the thickness of the active layer (P3HT:PCBM) and its light absorption play important roles in the determination of J_{SC} and absorption in the OSC structure. In addition, according to previous reports, the presence of metal nanoparticles can also increase the amount of absorption in OSC [24]. Therefore, the present study tries to improve the amount of these two quantities in the structure as much as possible by optimizing the thickness of the active layer and adding Al nanocylinders to it. First, to understand the effects of Al nanocylinders in two cases, i.e., with and without the presence of nanocylinders, the values are studied across different thicknesses of P3HT:PCBM active layer (50 nm-500 nm) (Fig. 5(a)). Then, we calculate the amount of absorption in terms of wavelength (300 nm-1200 nm) in the optimal thickness obtained (Fig. 5(b)). The hexagonal array pattern of nanocylinders is a structure with periodicity (p_x=p_y=21 nm), height (h=50 nm), and radius (r=10 nm).

As shown in Fig. 5, the incorporation of aluminum nanocylinders into the P3HT:PCBM active layer leads to a substantial enhancement in J_{SC}. In the absence of nanoparticles, J_{SC} increases only gradually with active layer thickness, consistent with the behavior of a conventional absorber. However, with nanocylinders present, J_{SC} peaks sharply at a thickness of 150 nm, beyond which it declines monotonically. This trend reflects the interplay between enhanced optical absorption and exciton dynamics: at 150 nm, the plasmonic near-field generated by the Al nanocylinders maximizes photon absorption and exciton generation (electron-hole pairs), while maintaining compatibility with the limited exciton diffusion length (~10 nm–20 nm) in P3HT:PCBM. For thicknesses exceeding 200 nm, J_{SC} decreases due to increased charge recombination losses, as photogenerated carriers fail to reach their respective electrodes before recombining.

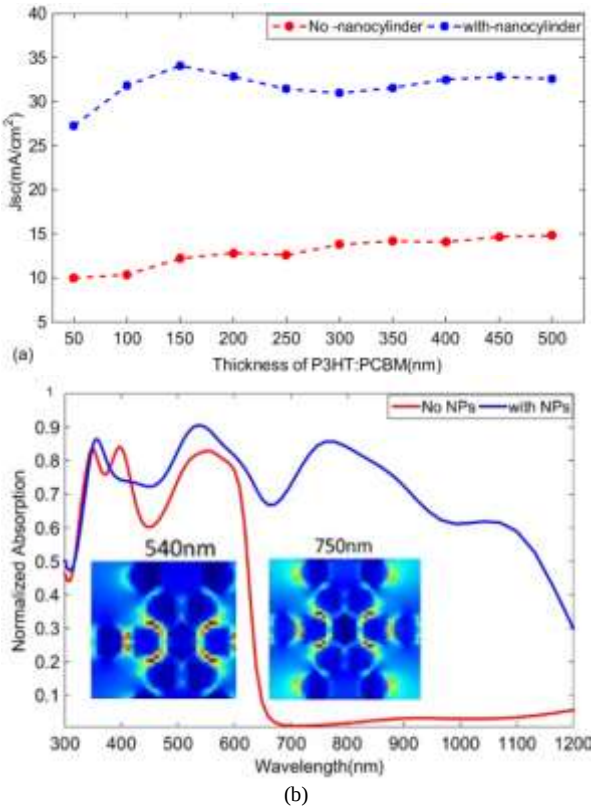

Fig. 5. (a) The diagram of the short circuit current density (J_{SC}) in terms of P3HT:PCBM thickness. (b) The absorption spectra for 150 nm thickness of P3HT:PCBM.

Figure 5(b) compares the optical absorption spectra, with and without nanocylinders, at the optimal 150 nm thickness across the 300 nm–1200 nm wavelength range. Without nanoparticles, absorption is confined to wavelengths below 650 nm, corresponding to the 1.9 eV bandgap of P3HT:PCBM, with negligible response in the near-infrared (NIR) region. The introduction of Al nanocylinders, however, introduces a secondary absorption mechanism driven by LSPR modes. These resonances, enabled by Al's broadband plasmonic response (UV to NIR) and non-zero imaginary refractive index, significantly enhance absorption both below and, crucially, above 650 nm. The enhancement arises from two primary mechanisms: (1) strong near-field localization between adjacent nanocylinders, which increases the effective absorption cross-section via dipole-dipole coupling; and (2) back-scattering of incident light toward the active layer, facilitated by the nanocylinders' proximity to the ZnO interface, thereby extending the optical path length. This dual effect effectively turns the nanocylinders into secondary light sources that amplify photon flux within the active layer.

Peak absorption values of 0.92 and 0.87 are observed at 540 nm and 740 nm, respectively, wavelengths that coincide with the plasmon resonance frequencies of the optimized nanostructure (see electric field distributions in Fig. 5(b)). These resonances are geometry-dependent and result from the collective oscillation of conduction electrons, which concentrate incident light into nanoscale volumes between particles. Consequently, the local electric field intensity, and thus the exciton generation rate, which scales quadratically with field strength, is amplified.

Given the strong dependence of plasmon resonance frequency on nanostructure geometry, precise control over the size and morphology of the Al nanocylinders provides an effective means to tailor plasmonic effects, thereby enhancing absorption and increasing J_{SC} in the OSC structure. To systematically evaluate the influence of nanocylinder dimensions on device performance, we first optimized the array periodicity, a critical parameter governing near-field interactions. As illustrated in Fig. 6, simulations were conducted for nanocylinders with a fixed height of 50 nm and radius of 10 nm embedded in a 150 nm-thick P3HT:PCBM active layer, while varying the array periodicity. The absorption spectra in the visible range exhibited minimal sensitivity to periodicity changes. In contrast, the infrared region displayed pronounced periodicity-dependent behavior, with maximal absorption achieved at a period of 21 nm. Beyond this optimal spacing, a gradual decline in absorption was observed. At small inter-particle distances (<8 nm), strong plasmonic gap modes emerged due to Coulomb coupling between surface charges on adjacent nanocylinders, resulting in intense field confinement within the nanogap. This field enhancement, which scales quadratically with electric field strength, significantly boosted photon absorption and exciton generation rates. As the periodicity increased, inter-particle coupling diminished, leading to weaker field localization and a convergence of the absorption trend toward that of a nanoparticle-without structure. These results underscore the essential role of periodicity in maximizing infrared absorption through inter-nanocylinder plasmonic coupling.

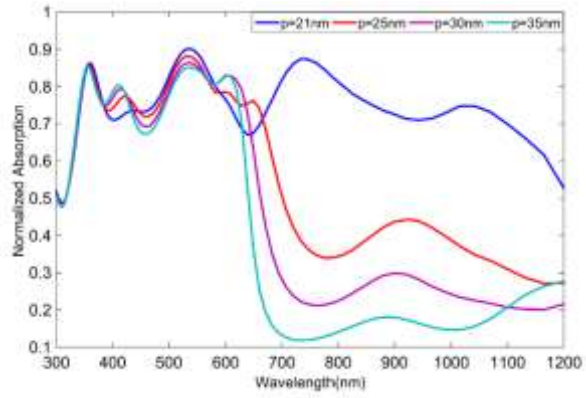

Fig. 6. The absorption spectra for different periods.

Upon determining the optimal periodicity of 21 nm, we systematically investigated the influence of Al nanocylinder dimensions on device performance. Figures 8(a) and 8(b) present the effects of nanocylinder height (50 nm, 100 nm, and 150 nm) on the short-circuit current density (J_{SC}) and absorption spectrum

across varying thicknesses of the P3HT:PCBM active layer and wavelengths. The results reveal that for each fixed nanocylinder height, there exists an optimal active layer thickness at which both J_{SC} and absorption reach their maximum values. This optimal thickness consistently demonstrates superior performance compared to other configurations, highlighting the critical interplay between nanocylinder geometry and active layer thickness in maximizing plasmonic enhancement. The observed trends underscore the importance of simultaneous optimization of both parameters for achieving optimal light harvesting and charge generation in plasmonic organic solar cells.

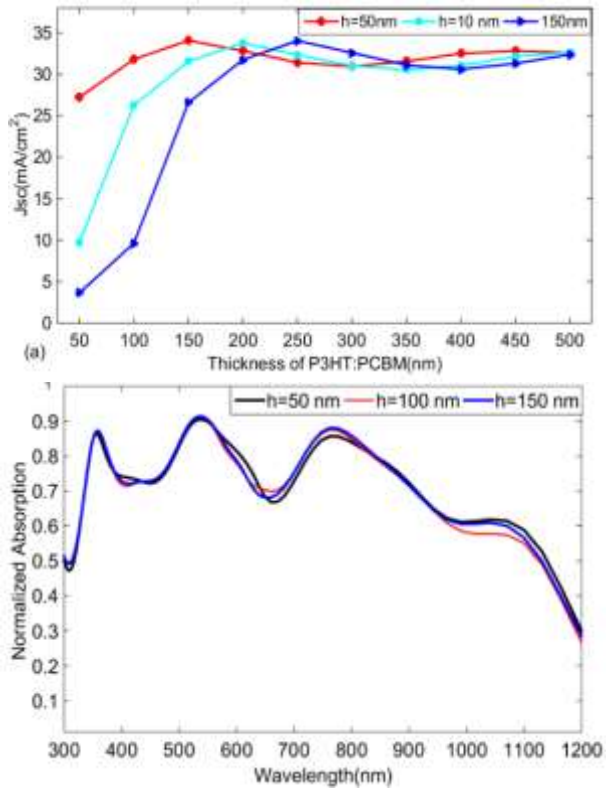

Fig. 7. (a). The J_{sc} diagram in terms of P3HT:PCBM thickness for 50, 100, and 150 nm heights. (b) The absorption spectra for heights of 50, 100, and 150 nm when the thickness of P3HT:PCBM is 150 nm.

As illustrated in Fig. 7(a), the optimal active layer thicknesses corresponding to nanocylinder heights of 50, 100, and 150 nm are 150 nm, 200 nm, and 250 nm, respectively, indicating a proportional relationship between nanocylinder height and the optimal P3HT:PCBM thickness. Although increasing the active layer thickness typically reduces J_{SC} due to limited charge carrier mobility and short exciton diffusion lengths, the incorporation of taller nanocylinders counteracts this effect by enhancing light scattering and internal reflection within the active layer. The increased volume ratio of nanocylinders prolongs light retention in the active layer, significantly extending the optical path length through intensified scattering. This enhanced light trapping improves the coupling of incident light into the active layer, thereby increasing both absorption and J_{SC}. The improved light coupling boosts photon absorption rates, leading to a higher probability of exciton generation. Furthermore, the LSPR-induced electromagnetic fields reduce exciton recombination and promote efficient charge carrier separation, contributing significantly to the enhancement of J_{SC}. The increase in absorption is partially attributable to the greater physical thickness of the active layer. These results demonstrate that the optimal P3HT:PCBM thickness is functionally dependent on nanocylinder height but independent of their radii.

After studying the role of the thickness of the P3HT:PCBM active layer in nanocylinders with constant height, in this step, we want to change the height of the nanoparticles (0, 50, 100, 150) at a fixed radius of 150 nm and check whether the maximum absorption value is obtained at the same height of 50 nm or not. At first, we comparatively calculated the diagram of the absorption spectrum in terms of wavelength state for different heights at a fixed radius of 10 nm (Fig. 8(a)). The results show the highest amount of absorption at a height of 50, which is more evident in the infrared regions. The peaks of the absorption spectrum are located in the near-UV-Vis regions and at wavelengths of 350 nm, 540 nm, and 740 nm.

As Fig. 8(a) shows, these peaks at optical wavelengths do not equally contribute to the increase of optical absorption despite localized surface plasmon (LSP) resonances. Compared to the case without nanoparticles, there is an evidently significant increase in absorption at a wavelength above 650 nm in the infrared region. This is caused by the fact that the LSPR of Al nanocylinders is located in the range of

visible and infrared spectra. As a result, the presence of these nanocylinders causes a fluctuating reduction in addition to increasing the absorption in these regions, compared to the state without nanoparticles.

Figure 8(b) shows the J_{SC} at different heights of nanocylinders. First, with the increase in height, the amount of J_{SC} increases, and then it will have a decreasing trend. Its maximum value is reached at a height of 50 nm, with an almost two-fold increase compared to the state without nanoparticles (14.07 mA/cm^2), that is, 34.06 mA/cm^2. This value is a significant improvement on those reported by the studies that have been done so far [41]. At this optimal height, it can be stated that the reflection of photons to buffer layers is reduced by nanocylinders. As a result, more photon energy is transferred to the active layer by light localizing in the presence of spectral overlap between Al nanocylinders and P3HT:PCBM [44]. There will be an increase in the number of electric charge carriers produced in the active layer by reducing the energy losses, due to the coupling of plasmonic modes and the more localized near-field distribution of the nanocylinders. As a result, the amount of J_{sc} and absorption at the height of 50 nm is improved, as compared to other sizes. By increasing the height of the nanocylinders (150 nm), the coupling will be weakened between the LSP modes of the nanocylinders and the incident light photons in the active layer, and as a result, the amount of J_{SC} will be reduced in the active layer.

In addition, it can be stated that as the height increases, a large amount of incident light will be absorbed by nanocylinders, and a smaller amount of light will enter the active layer. Therefore, the decrease in absorption can be attributed to the larger volume of nanocylinders as well as the destructive interference of light scattered by them.

As shown in Fig. 9(b), no significant difference is observed at lower wavelengths (420 nm-350 nm) between the absorption spectrum plots, because in these regions, nanocylinders do not have strong absorption, compared to the state without nanoparticles (see Fig. 5). Therefore, the presence or absence of nanoparticles does not cause much change in absorption spectrum curves. In the calculations, nanocylinders with a radius of 20 nm have a lower absorption. It can be explained that the nanocylinders act as a mirror for the incident light, as this radius, and therefore, they prevent light from entering the active layer, weakening the transmission field to some extent [44]. In addition, at a radius of 15 nm, the increase of J_{SC} and absorption can be a reason for the effective coupling between incident light radiation photons and the nanocylinder LSP, and between the incident light photons and the active layer. Moreover, the rate of exciton production, which is proportional to the square of the intensity of the alternating field, increases at this radius.

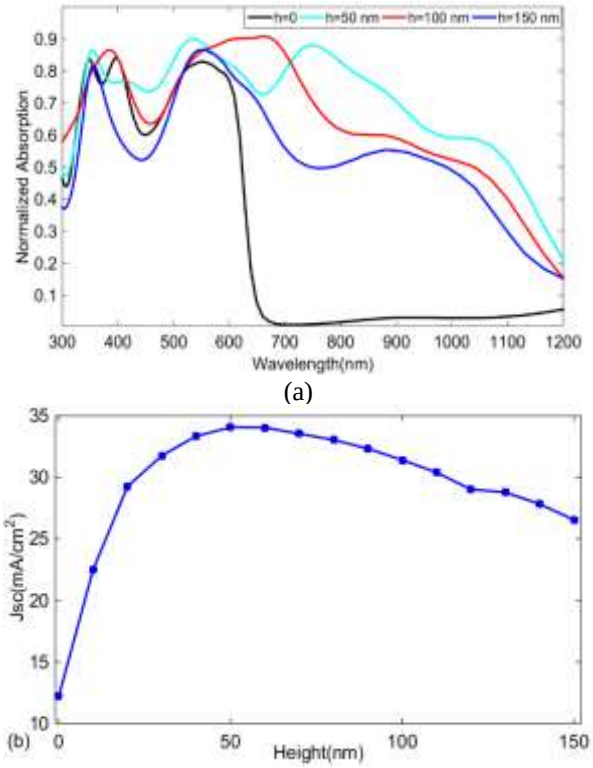

Fig. 8. (a) The absorption spectra at heights of 0, 50, 100, and 150 nm for nanocylinders in a 150 nm thickness of P3HT:PCBM. (b) The short circuit current density diagram in terms of the heights of nanocylinders in a 150 nm thickness of P3HT:PCBM.

The present study deals with the influence of another characteristic of nanocylinders, namely their radii, on J_{SC} and absorption quantities. First, we calculate J_{SC} changes in terms of height (10 nm-150 nm) in different radii (5 nm,

10 nm, 15 nm, 20 nm) (Fig. 9(a)). The diagrams show that as the radius increases, the values of J_{SC} and absorption will increase, and they find a decreasing trend in the radius of 20 nm. The calculations show that when the radius of the nanocylinders reaches 15 nm at a height of 50 nm, J_{SC} will have its highest value, i.e., 36.04 mA/ cm^2 . After that, the value of J_{sc} will decrease as the radius increases. In general, in accordance with the stated relationships, absorption dominates scattering in nanoparticles with a size smaller than 50 nm [17]. Given the dimensions, therefore, small metal nanocylinders act as subwavelength antennas. The plasmonic near field in nanocylinders is coupled with the active layer, and as a result, the effective absorption cross-section and exciton dissociation increase.

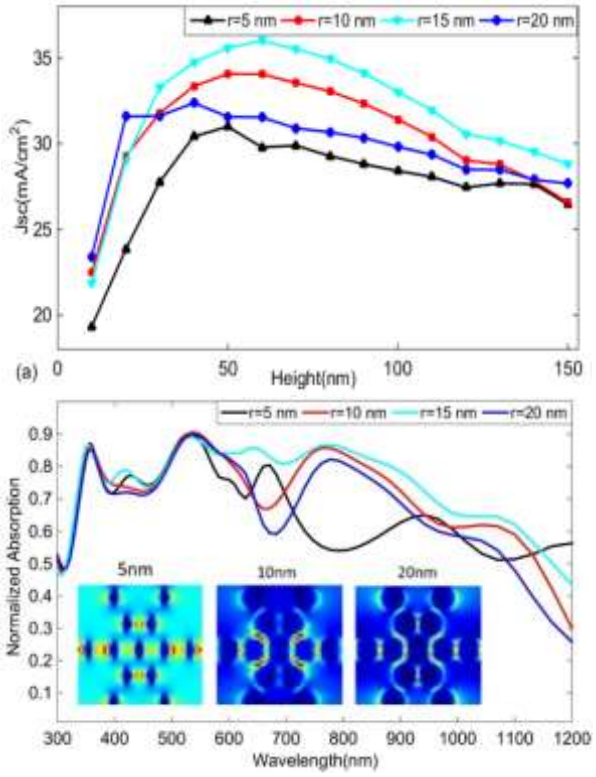

(b)

Fig. 9. (a) The diagram of J_{SC} in terms of heights at fixed radii of 5, 10, 15, and 20 nm. (b) The absorption spectra at constant radii of 5, 10, 15, and 20 nm.

We showed the distribution of the field at the radii of 5, 10, and 20 nm at the wavelength of 750 nm, where the main difference can be observed in the peaks of the absorption spectrum (Fig. 9). The results show, that the intensity of LSP resonances at the radius of 10, and 20 nm is lower than the radius of 15 nm and that the intensity at the radius of 5nm is not strong enough to completely enter the active layer. Therefore, to have a better understanding of the absorption peaks at the radius of 15 nm at the wavelengths of λ_1=350 nm, λ_2=540 nm, and λ_3 =750 nm, we showed their field distribution shapes in three planes, i.e., x-y, y-z, and x-z planes (Fig. 10). In the above wavelengths, given the presence of plasmonic effects due to the high localization of light energy in the nanoscale space, the electromagnetic field increases in the distances between the nanocylinders and their side and surface cross-sections.

It should be noted that the reported J_{SC} (36.04 mA/cm²) represents a theoretical optical upper bound calculated solely based on the enhanced absorption spectra under the ideal assumption of a 100% EQE. This value is significantly higher than the experimentally reported J_{SC} values for P3HT:PCBM-based organic solar cells, which typically fall within the range of 9–12 mA/cm² for conventional devices [45], [46] and can increase up to approximately 12–18 mA/cm² in optimized structures incorporating plasmonic nanoparticles, yet still remain below the theoretical optical limit [47]- [49].

This discrepancy mainly arises from the intrinsic physical limitations of the P3HT:PCBM system, including the short exciton diffusion length [50], [51] and carrier recombination losses [52], which are discussed in the following section. Therefore, the reported value should be interpreted as an optical upper bound resulting from enhanced light absorption through LSPR modes and increased effective optical path length, rather than as a direct prediction of the actual device performance.

Building upon this optical analysis, the geometric optimization indicates that the maximum J_{SC} is obtained for an aluminum nanocylinder array with a periodicity of 21 nm and a radius of 15 nm, where strong LSPR excitation in the near-infrared region maximizes absorption enhancement. However, achieving interparticle gaps below 20 nm involves considerable fabrication challenges,

particularly for scalable techniques such as colloidal lithography or thermal/UV nanoimprint lithography [53]. Nevertheless, advanced nanofabrication methods such as block-copolymer lithography, anodic aluminum oxide (AAO) templating, and high-resolution nanoimprint techniques have enabled the realization of sub-30-nm periodic patterns. At these length scales, nonlocal effects may induce minor shifts in the resonance position or linewidth; however, hydrodynamic models indicate that these deviations remain small, and classical electromagnetic descriptions retain sufficient accuracy. Furthermore, quantum-size effects typically become significant only when feature dimensions approach 2 nm–5 nm, and therefore are not expected to play a dominant role for the larger dimensions employed in this work. [53]. To bridge the gap between theoretical optimization and experimental feasibility, additional FDTD simulations were conducted using more practical geometrical parameters. As summarized in Table 1, increasing the periodicity to 50 nm–80 nm (corresponding to interparticle gaps of 20 nm–50 nm for radii of 15–30 nm) reduces the optical upper-limit J_{SC} to 20.8–29.8 mA/cm². Despite this reduction, even the most experimentally accessible configuration (P=80 nm, r=30 nm) yields approximately 48% higher absorption than the reference cell without nanoparticles (14.07 mA/cm²). For intermediate periodicities of 50 nm–60 nm, which are readily achievable using established nanolithography techniques, a substantial enhancement of approximately 112% is preserved. The observation of such significant improvement within experimentally attainable dimensions confirms the practical relevance of the proposed plasmonic design for enhancing near-infrared light harvesting and improving the performance of organic photovoltaic devices.

In the last step of calculations, in the optimized OSC structure, the effect of the incident light angle on the absorption and scattering rates in the active layer was studied, as shown in Fig. 11. The results show that the amount of light absorption in the active layer of the P3HT:PCBM solar cell is affected by the angle of incident light. With a gradual increase in the angle of incidence, in addition to the visible spectral region, a significant decrease in the amount of light absorption is observed in the infrared region (wavelengths above 700 nm).

In explaining the results, it can be stated that at oblique angles of irradiation, due to the reduction in the direct effect of light on aluminum nanocylinders, their efficiency in trapping and absorbing light decreases. Also, at larger angles of incidence, light scattering in the surface layer increases, and its penetration into the depth of the solar cell decreases, especially in the infrared region. As a result of these processes, the plasmonic resonance conditions of the Al nanocylinders have changed in the active layer, leading to a decrease in light absorption by the active layer.

Table 1. FDTD-simulated optical J_{SC} for Al nanocylinder arrays with varying radius and periodicity.

Period (nm)	Radius (nm)	Gap (nm)	J_{SC} (mA/cm²)
50	15	20	29.8
50	20	10	27.5
60	15	30	28.5
60	20	20	26.2
60	25	10	24.0
70	15	40	26.8
70	20	30	25.1
70	25	20	23.5
70	30	10	21.0
80	15	50	24.5
80	20	40	23.8
80	25	30	22.5
80	30	20	20.8

Although the optical simulations performed for the proposed structure demonstrate a significant enhancement in light absorption, particularly in the NIR region, it should be emphasized that the conversion of this enhanced absorption into a realistic photocurrent is governed by three fundamental physical limitations: the exciton diffusion length, carrier recombination processes, and interactions with metallic nanostructures. The exciton diffusion length in P3HT:PCBM systems is typically reported to be in the range of 10 nm–20 nm [54], implying that only excitons generated in close proximity

to the donor–acceptor interface can effectively dissociate into free charge carriers before recombination. The electric field distribution (Fig. 10) indicates that plasmonic enhancement near the surface of the nanocylinders leads to a substantial increase in optical absorption and the formation of intense localized field regions ("plasmonic hot spots"). However, the spatial overlap between these enhanced absorption regions and the exciton harvesting zone can only partially compensate for the limitation imposed by the short exciton diffusion length. In practice, a considerable fraction of the generated excitons undergoes bimolecular non-radiative recombination prior to dissociation, due to limited carrier mobility and inefficient charge transport.

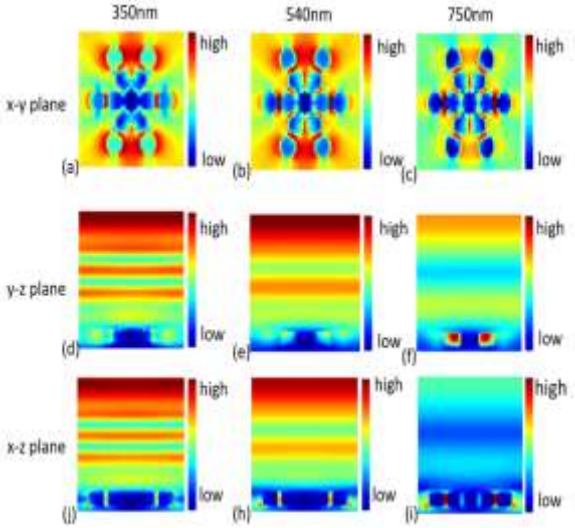

Fig. 10. The distribution of the electric fields in the solar cell at wavelengths of 350, 540, and 750 nm. (a-c) in the x-y plane. (d-f) in the y-z plane. (j-i) in the x-z plane

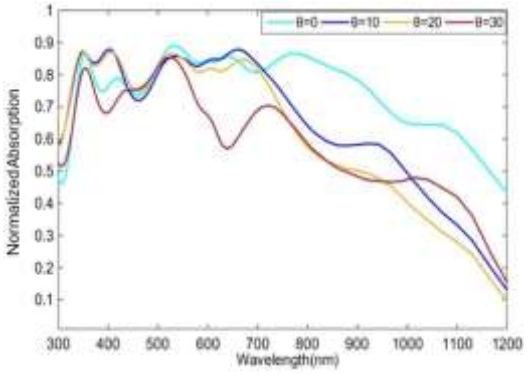

Fig. 11. Absorption spectra at different incidence angles.

Beyond these photophysical limitations, electrical losses associated with high series resistance (R_s), which hinders charge extraction, and low shunt resistance (R_{sh}), which introduces leakage pathways, can reduce the fill factor (FF) and open-circuit voltage (V_{oc}), thereby limiting charge-extraction efficiency and lowering the practical photocurrent relative to the optical limit. In addition, carrier recombination, particularly non-radiative processes, can further suppress the efficiency of exciton dissociation and charge collection, increasing the mismatch between absorbed photons and extractable carriers. Moreover, the presence of metallic nanostructures near the active layer (Fig. 1(b)) may induce non-radiative energy transfer from excitonic dipoles to the metal through near-field coupling with its electronic modes, including surface plasmon modes, leading to metal-induced quenching and reduced exciton dissociation efficiency. However, the electric-field distribution (Fig. 10) indicates that the plasmonic near-field enhancement around the nanoparticles, particularly at a wavelength of 750 nm, largely compensates for these non-radiative losses. This observation is consistent with experimental studies, which show that at metal–semiconductor separations of 5 nm–15 nm, enhanced optical absorption can dominate over metal-induced quenching [55]. Furthermore, the choice of Al is advantageous, as its interband transition threshold at 1.5 eV [56] and relatively low ohmic damping in the near-infrared region reduce plasmonic losses compared with noble metals.

Overall, these combined optical, excitonic, and electrical limitations clarify why the plasmon-enhanced absorption achieved in our design does not directly translate into a proportional increase in the experimentally measurable photocurrent. For accurate quantitative prediction of device behavior, it is crucial to combine optical simulation results with charge transport models, such as the Pettersson model [57] or drift–diffusion simulations; therefore, employing this approach is recommended in future studies.

IV. CONCLUSION

This study demonstrates that embedding a hexagonal array of plasmonic aluminum nanocylinders within the P3HT:PCBM active layer is a highly effective strategy for enhancing near-infrared (NIR) absorption in organic solar cells. Through systematic finite-difference time-domain (FDTD) simulations, we optimized the nanostructure geometry, including nanocylinder height (50 nm), radius (15 nm), and array period (21 nm), to maximize light harvesting in the critical 650 nm–1200 nm spectral range, where P3HT:PCBM exhibits inherently weak absorption. The optimized design achieves a remarkable optical upper bound J_{SC} of 36.04 mA/cm², representing a twofold enhancement over the reference cell without nanoparticles. This substantial improvement is attributed to the strong coupling of localized surface plasmon resonance (LSPR) modes, which significantly intensify the near-field distribution and extend the effective optical path length within the active layer, particularly in the NIR region. Furthermore, our results reveal that the optimal active layer thickness (150 nm) is directly correlated with nanocylinder height, ensuring a balance between enhanced photon absorption and efficient exciton collection. Crucially, aluminum's unique inter-band transitions enable plasmonic activity deep into the NIR, making it an ideal, low-cost alternative to noble metals. This work establishes aluminum (Al) nanocylinders as a scalable and high-performance plasmonic platform for next-generation organic photovoltaics, offering a promising optical strategy to mitigate the NIR absorption bottleneck in organic solar cells.

ACKNOWLEDGMENT

The authors would like to thank Shahid Chamran University of Ahvaz and Lorestan University for supporting this work.

REFERENCES

[1] Y.F. Li, Z.L. Kou, J. Feng, and H.B. Sun, "Plasmon-enhanced organic and perovskite solar cells with metal nanoparticles," J. Nanophotonics. Vol. 9, pp. 3111-3133, 2020.

[2] J. Rivera-Taco, R. Castro Beltra´n, J.L. Maldonado, J. A´lvarez Martı´nez, D. Barreiro Argu¨elles, J.A. Gaspar, and G. Gutie´rrez Jua´rez, "The Role of Silver Nanoparticles in the Hole Transport Layer in Organic Solar Cells Based on PBDB-T: ITIC," Electron. Mater., Vol. 50, pp. 4118-4127, 2021.

[3] M. Notarianni, K. Vernon, A. Chou, J. Liu, and N. Motta, "Plasmonic effect of annealed gold islands for improving the efficiency of organic solar cells," Adv. Device Mater., Vol. 1, pp. 27-32, 2015.

[4] Z. Xia, T. Song, J. Sun, S.T. Lee, and B. Sun, "Plasmonic enhancement in hybrid organic/Si heterojunction solar cells enabled by embedded gold nanoparticles," Appl. Phys. Lett., Vol 105, pp. 241110(1-5), 2015.

[5] S.W. Baek, G. Park, J. Noh, C. Cho, C.H. Lee, M.K. Seo, H. Song, and J.Y. Lee, "Au@ Ag core–shell nanocubes for efficient plasmonic light scattering effect in low bandgap organic solar cells," ACS Nano, Vol. 8, pp. 3302-3312, 2014.

[6] V. Mann and V. Rastogi, "FDTD simulation studies on improvement of light absorption in organic solar cells by dielectric nanoparticles," Opt. Quant Electron., Vol. 52, pp. 233(1-16), 2020.

[7] J. Wang, S. Jia, Y. Cao, W. Wang, and P. Yu, "Design principles for nanoparticle plasmon-enhanced organic solar cells," Nanoscale Res. Lett., Vol. 13, pp. 211(1-6), 2018.

[8] M.Z. Islam, F. Snigdha, and M.S. Hasan, "Plasmonically-enhanced absorption in organic solar cells with metal nanostructures," 2018 9th International Renewable Energy Congress (IREC), IEEE, pp. 1-5, 2018.

[9] S. Mohapatra, T.A. Nguyen, and P. Nguyen-Tri, *Noble Metal-Metal Oxide Hybrid Nanoparticles*, Elsevier, 2019.

[10] M. Socol and N. Preda, "Hybrid Nanocomposite Thin Films for Photovoltaic Applications: A Review," Nanomaterials, Vol. 11, pp. 1117(1-48), 2021.

[11] D. Rourke, S. Ahn, A.M. Nardes, J. Van De Lagemaat, N. Kopidakis, and W. Park, "Integrated optical and electrical modeling of plasmon-enhanced thin film photovoltaics: A case-study on organic devices," Appl. Phys., Vol. 116, pp. 11451-11751, 2014.

[12] M. Rassekh, R. Shirmohammadi, R. Ghasempour, F.R. Astaraei, and S.F. Shayesteh, "Effect of plasmonic Aluminum nanoparticle shapes on optical absorption enhancement in silicon thin-film solar cells," Phys. Lett. A, Vol. 408, pp. 127509(1-10), 2021.

[13] A.S. Mohsin, M. Mobashera, A. Malik, M. Rubaiat, and M. Islam, "Light trapping in thin-film solar cell to enhance the absorption efficiency using FDTD simulation," J. Opt., Vol. 49, pp. 523-532, 2020.

[14] H. Heidarzadeh and A. Tavousi, "Design of an LSPR-Enhanced Ultrathin CH3NH3PbX3 Perovskite Solar Cell Incorporating Double and Triple Coupled Nanoparticles," Electron. Mater., Vol. 50, pp. 1817-1826, 2021.

[15] M.A. Alkhalayfeh, A.A. Aziz, and M.Z. Pakhuruddin, "An overview of enhanced polymer solar cells with embedded plasmonic nanoparticles," Renew. Sustain. Energy Rev., Vol. 141, pp. 110726(1-48), 2021.

[16] K.A. Catchpole and A. Polman, "Plasmonic Solar Cells," Opt. Express, Vol. 16, pp. 21793-21800, 2008.

[17] A. Elrashidi and K. Elleithy, "High Performance Polymer Solar Cells Using Grating Nanostructure and Plasmonic Nanoparticles," Polymers, Vol. 14, pp. 862(1-12), 2022.

[18] E.L. Lim, C.C. Yap, M. Asri, and M.A.M. Teridi, "A review of recent plasmonic nanoparticles incorporated P3HT:PCBM organic thin film solar cells," Org. Electron., Vol. 36, pp. 12-28, 2016.

[19] G.P. Singh and N. Sardana, "Plasmonic response of metallic nanoparticles embedded in glass and a-Si," Bull. Mater. Sci., Vol. 45, pp. 241(1-9), 2022.

[20] C.F. Bohren and D.R. Huffman, *Absorption and scattering of light by small particles*, John Wiley & Sons, p. 544, 2008.

[21] J.J. Zhang, Z.G. Qu, J.F. Zhang, and A. Maharjan, "A three-dimensional numerical study of coupled photothermal and photoelectrical processes for plasmonic solar cells with nanoparticles," Renew. Energy, Vol. 165, pp. 278-287, 2021.

[22] G. Singh, J.S. Sekhon, and S.S. Verma, "Enhanced photocurrent in thin-film GaAs solar cells with embedded Al nanoparticles," Energy Sources A: Recovery Util. Environ. Eff., Vol. 42, pp. 815-823, 2020.

[23] A. Yang, A.J. Hryn, M.R. Bourgeoisb, W.-K. Lee, J. Hu, G.C. Schatz, and T.W. Odom, "Programmable and reversible plasmon mode engineering," Proceedings of National Academy of Sciences (PNAS) of U.S.A., Vol. 113, pp. 14201-14206, 2016.

[24] P. Liu, S.E. Yang, J. Han, Y. Ma, Y. Jia, and Y. Chen, "Research of Ag nanospheres for absorption enhancement in amorphous silicon thin film solar cells," J. Opt., Vol. 46, pp. 265-268, 2017.

[25] P.R. Pudasaini and A.A. Ayon, "High efficiency nanotextured silicon solar cells," Opt. Commun., Vol. 285, pp. 4211-4212, 2012.

[26] K. Kumar, A. Das, U.K. Kumawat, and A. Dhawan, "Tandem organic solar cells containing plasmonic nanospheres and nanostars for enhancement in short circuit current density," Opt. Express, Vol. 27, pp. 31599-31620, 2019.

[27] W.H. Tseng, C.Y. Chiu, S.W. Chou, H.C. Chen, M.L. Tsai, Y.C. Kuo, D.H. Lien, Y.C. Tsao, K.Y. Huang, C.T. Yeh, J.H. He, C.I. Wu, M.H. Huang, and P.T. Chou, "Shape-dependent light harvesting of 3D gold nanocrystals on bulk heterojunction solar cells: plasmonic or optical scattering effect?" Phys. Chem. C, Vol. 119, pp. 7554-7564, 2015.

[28] Y.-S. Hsiao, S. Charan, F.-Y. Wu, F.-C. Chien, C.-W. Chu, P. Chen, and F.-C. Chen, "Improving the light trapping efficiency of plasmonic polymer solar cells through photon management," Phys. Chem. C, Vol. 116, pp. 20731-20737, 2012.

[29] A.S. Mahdi, L.M. Shaker, and A. Alamiery, "Recent advances in organic solar cells: materials, design, and performance," J. Opt., Vol. 53, pp. 1403-1419, 2024.

[30] F. Enrichi, A. Quandt, and G.C. Righini, "Plasmonic enhanced solar cells: Summary of possible strategies and recent results," Renew. Sust. Energ. Rev., Vol. 82, pp. 2433-2439, 2018.

[31] R. Kroon, M. Lenes, J.C. Hummelen, P.W. Blom, and B. De Boer, "Small bandgap polymers for organic solar cells (polymer material development in the last 5 years)," Polym. Eng. Rev., Vol. 48, pp. 531-582, 2008.

[32] S.R. Rodriguez, A. V. Kabashin, W.L. Barnes, and A.N. Grigorenko "Breaking the symmetry of forward-backward light emission with localized and collective magnetoelectric resonances in arrays of pyramid-shaped aluminum nanoparticles," Phys. Rev. Lett., Vol. 113, pp. 247401(1-5), 2014.

[33] M. Que, Z. Zhang, J. Qin, W. Shi, Y. Liu, Y. Zhang, Y. Liu, H. Gao, and Y. Mao, "Enhanced conversion efficiency in perovskite solar cells by effectively utilizing near-infrared light," Nanoscale, Vol. 8, pp. 14432-14437, 2016.

[34] J.R. Tumbleston, D.H. Ko, E.T. Samulski, and R. Lopez, "Electrophotonic enhancement of bulk heterojunction organic solar cells through photonic crystal photoactive layer," Appl. Phys. Lett., Vol. 94, pp. 043305(1-5), 2009.

[35] S. Kasani, K. Curtin, and N. Wu, "A review of 2D and 3D plasmonic nanostructure array patterns: fabrication, light management and sensing applications," Nanophotonics, Vol. 8, pp. 2065-2089, 2019.

[36] M. Shaban, M. Benghanem, A. Almohammedi, and M. Rabia, "Optimization of the active layer P3HT: PCBM for organic solar cell," Coatings, Vol. 11, pp. 863(1-15), 2021.

[37] A.K. Verma, N. Shukla, and S. Tiwari, "Effect of ZnO ETL and MoO_3 HTL with PCDTBT:PC_{70}BM-based BHJ organic solar cells," Nanomater Energy, Vol. 9, pp. 1800021(1–8), 2020.

[38] S.M. Hasheminassab, M. Imanieh, A. Kamali, S.A. Emamghorashi1, and S. Hassanhossein, "Influence of the shape and size of Ag nanoparticles on the performance enhancement of CIGS solar cells: the role of surface plasmons," Plasmonics, Vol. 16, pp. 273-282, 2021.

[39] W. Rene, G. Zhang, Y. Wu, H. Ding, Q. Shen, K. Zhang, J. Li, Nan Pan, and X. Wang, "Broadband absorption enhancement achieved by optical layer mediated plasmonic solar cell," Opt. Express, Vol. 19, pp. 26536-26550, 2011.

[40] F. Sobhani, H. Heidarzadeh, and H. Bahador, "Efficiency enhancement of an ultra-thin film silicon solar cell using conical-shaped nanoparticles: similar to superposition (top, middle, and bottom)," Opt. Quantum Electron., Vol. 52, pp. 387(1-13), 2020.

[41] A. Uddin and X. Yang, "Surface plasmonic effects on organic solar cells," Nanoscience Nanotechnol., Vol. 14, pp. 1099-1119, 2014.

[42] A. Taflove, S.C. Hagness, and M. Piket-May, *Computational electromagnetics: the finite-difference time-domain method*, Elsevier, 2005.

[43] H. Jia, C.C. Tsoi, A.E. Abed, and W. Yu, "Metallic plasmonic nanostructure arrays for enhanced solar photocatalysis," Laser Photonics Rev., Vol. 17, pp. 2200700(1-38), 2023.

[44] T.T. Zygiridis, "A Short Review of FDTD-Based Methods for Uncertainty Quantification in Computational Electromagnetics," Math. Probl. Eng., Vol. 2017, pp. 9247978(1-8), 2017.

[45] S. Anjusree, K.R. Arya, and C.D. Bikas., "Air-processed active-layer of organic solar cells investigated by conducting AFM for precise defect detection," RSC Adv., Vol. 10, pp. 24882-24892, 2020.

[46] B. Kadem, A. Hassan, M. Göksel, T. Basova, A. Şenocak, E. Demirbaş, and M. Durmuş, "High performance ternary solar cells based on P3HT: PCBM and ZnPc-hybrids," RSC Adv., Vol. 6, pp. 93453-93462, 2016.

[47] M. Omrani, H. Fallah, K.L. Choy, and M. Abdi-Jalebi, "Impact of hybrid plasmonic nanoparticles on the charge carrier mobility of P3HT: PCBM polymer solar cells," Sci. Rep., Vol. 11, pp. 19774(1-14), 2021.

[48] A. Ali, F. El-Mellouhi, A. Mitra, and B. Aïssa, "Research progress of plasmonic nanostructure-enhanced photovoltaic solar cells," Nanomater., Vol. 12, pp. 788(1-46), 2022.

[49] M.A. Ibrahem, B.G. Rasheed, B. Canimkurbey, A.M. Adawi, J.S.G. Bouillard, and M. O'Neill, "Improving the Efficiency of Bulk-heterojunction Solar Cells through Plasmonic Enhancement within a Silver Nanoparticle-Loaded Optical Spacer Layer," ACS Omega, Vol. 10, pp. 2849-2857, 2025.

[50] D. Gupta, T.G. Hofstad, R.A. Janssen, and S.C. Meskers, "Evidence for exciton quenching by hole polarons in thick P3HT:PCBM solar cells," In Conference Proceedings, ICEE2016 pp. 1-4, 2016.

[51] D. Rana, V. Jovanov, V. Wagner, A. Materny, and P. Donfack, "Insights into ultrafast charge-pair dynamics in P3HT: PCBM devices under

the influence of static electric fields," RSC Adv., Vol. 10, pp. 42754-42764, 2020.

[52] L.J.A. Koster, M. Kemerink, M.M. Wienk, K. Maturová, and R.A. Janssen, "Quantifying bimolecular recombination losses in organic bulk heterojunction solar cells," Adv. Mater., Vol. 23, pp. 1670-1674, 2011.

[53] J. Yang, M. Zhang, X. Lan, X. Weng, Q. Shu, R. Wang, and Y. Yang, "Controllable fabrication of non-close-packed colloidal nanoparticle arrays by ion beam etching," Nanoscale Res. Lett., Vol. 13, pp. 177(1-11), 2018.

[54] C. Deibel, and V. Dyakonov, "Polymer–fullerene bulk heterojunction solar cells," Rep. Prog. Phys., Vol. 73, pp. 096401(1-39), 2010.

[55] D.H. Ko, J.R. Tumbleston, L. Zhang, S. Williams, M.J. Eisner, M.C. Weisz, J.M. DeSimone, and E.T. Samulski, "Light-trapping in polymer solar cells by intentional surface roughness," Adv. Funct. Mater., Vol. 20, pp. 2461–2469, 2010.

[56] M.W. Knight, N.S. King, L. Liu, H.O. Everitt, and A.V. Kildishev, "Aluminum for plasmonics," ACS nano, Vol. 1, pp. 1–7, 2014.

[57] L.A.A. Patterson, "Modeling photocurrent action spectra of photovoltaic devices based on organic thin films," Appl. Phys., Vol. 86, pp. 487–496, 1999.

Nasrin Sepahvand received her B.Sc. degree in Applied Physics from Khorramabad Azad University, Khorramabad, Iran, in 2007, her M.Sc. degree in Atomic and Molecular Physics from Lorestan University, Iran, in 2018. She completed her Ph.D. in Optics and Laser at Shahid Chamran University of Ahvaz, Ahvaz, Iran, in 2024.

Abdolmohammad Ghalambor Dezfuli received his B.Sc. degree in Physics from Shahid Chamran University of Ahvaz, Ahvaz, Iran. He obtained his M.Sc. in spectroscopy laser and Ph.D degrees mass specroscopy from McGill University, Canada. He is currently an associate professor of physics at Shahid Chamran University of Ahvaz. His main research interests include nanofibers, optical properties of materials, spectroscopy, and laser-matter interaction.

Mohsen Bahrami received his B.Sc. degree in physics from Birjand University, Birjand, Iran, M.Sc. in atomic and molecular physics (laser) from Shahid Beheshti University, Tehran, Iran, and PhD in Photonics from Laser and Plasma Research Institute, Shahid Beheshti University. He is currently an assistant professor at Lorestan University, Khorramabad, Iran. His main research interests are Biophotonics, light-matter interaction and electrical charge and light transfer in different media.